J. metamorphic Geol., 2004, **22,** 1–15 doi:10.1111/j.1525-1314.2003.00492.x

Metamorphic evolution of garnet-bearing ultramafic rocks from the Gongen area, Sanbagawa belt, Japan

M. ENAMI,[1] T. MIZUKAMI[1,2] AND K. YOKOYAMA[3]
[1]*Department of Earth and Planetary Sciences, Nagoya University, Chikusa-ku, Nagoya 464–8602, Japan (enami@eps.nagoya-u.ac.jp)*
[2]*Department of Geology and Mineralogy, Kyoto University, Sakyo-ku, Kyoto 606–8502, Japan*
[3]*Department of Geology and Paleontology, National Science Museum, Shinjyuku-ku, Tokyo 169–0073, Japan*

ABSTRACT Garnet-bearing ultramafic rocks including clinopyroxenite, wehrlite and websterite locally crop out in the Higashi-akaishi peridotite of the Besshi region in the Cretaceous Sanbagawa metamorphic belt. These rock types occur within dunite as lenses, boudins or layers with a thickness ranging from a few centimetres to 1 metre. The wide and systematic variation of bulk-rock composition and the overall layered structure imply that the ultramafic complex originated as a cumulate sequence. Garnet and other major silicates contain rare inclusions of edenitic amphibole, chlorite and magnetite, implying equilibrium at relatively low *P–T* conditions during prograde metamorphism. Orthopyroxene coexisting with garnet shows bell-shaped Al zoning with a continuous decrease of Al from the core towards the rim, consistent with rims recording peak metamorphic conditions. Estimated *P–T* conditions using core and rim compositions of orthopyroxene are 1.5–2.4 GPa/700–800 °C and 2.9–3.8 GPa/700–810 °C, respectively, implying a high *P/T* gradient (> 3.1 GPa/100 °C) during prograde metamorphism. The presence of relatively low *P–T* conditions at an early stage of metamorphism and the steep *P/T* gradient together trace a concave upwards *P–T* path that shows increasing *P/T* with higher *T*, similar to *P–T* paths reported from other UHP metamorphic terranes. These results suggest either (1) down dragging of hydrated mantle cumulate parallel to the slab–wedge interface in the subduction zone by mechanical coupling with the subducting slab or (2) ocean floor metamorphism and/or serpentinization at early stage of subduction of oceanic lithosphere and ensuing HP–UHP prograde metamorphism.

Key words: Besshi region; garnet; geothermobarometer; orthopyroxene; *P–T* trajectory; Sanbagawa belt; ultra-high pressure metamorphism; ultramafic rocks.

INTRODUCTION

Garnet-bearing ultramafic (GUM) rocks have been reported from many orogenic belts. Most occur in high-pressure (HP) and ultrahigh-pressure (UHP) terranes in continent-continent collision zones (e.g. Brueckner & Medaris, 2000). Moreover, rare and significant GUM rocks also occur in HP or UHP metamorphic belts of island arcs such as the Sanbagawa belt (Mori & Banno, 1973; Kunugiza *et al.*, 1986) and Sulawesi Island (Kadarusman & Parkinson, 2000). The Sulawesi GUM rocks and associated UHP metamorphic rocks are considered to have formed related to continent–continent collision processes which predated island arc development. Thus the Sanbagawa samples are probably a unique example of GUM rocks related to the oceanic subduction.

GUM rocks in HP or UHP metamorphic belts can be interpreted in the following ways: (1) high *P/T* grade products of subduction metamorphism of ultramafic rocks previously presented in the crust or their serpentinized equivalents (Ernst, 1978; Evans & Trommsdorff, 1978; Jamtveit, 1987); (2) relics of ancient subducted lithosphere in the upper mantle (Carswell *et al.*, 1983; Brueckner & Medaris, 1998); or (3) mantle wedge materials transferred to the subducted slab during subduction or subsequent collision (Medaris *et al.*, 1995; Zhang *et al.*, 2000). GUM rocks contain valuable information needed to gain a better understanding of the tectonic evolution of convergent margins and material recycling in the crust-mantle system. One effective strategy for testing possible models for these large-scale geological phenomena is to establish the *P–T–t* paths of the HP–UHP GUM rocks using mineralogical and textural data. This can be difficult because most of the GUM rocks have been recrystallized during exhumation and now record little information on the subduction stage (Zhang *et al.*, 1994; Altherr & Kalt, 1996). The *P–T* evolution during the prograde stage is therefore commonly reconstructed by linking *P–T* estimates for different samples from different localities (e.g. Zhang *et al.*, 2000). However, such *P–T* arrays do not necessarily correspond to *P–T* paths of individual rocks, which is needed to gain a real understanding of the metamorphic evolution of a given region.

The geology and petrology of the GUM rocks of the Higashi-akaishi mass in the Sanbagawa belt were first

described by Horikoshi (1937). Subsequently Banno (1968, 1970) and Ernst *et al.* (1970) used Fe–Mg partitioning between garnet-clinopyroxene to suggest that the equilibrium temperatures of the GUM rocks are equivalent to the epidote–amphibolite and/or amphibolite facies. Mori & Banno (1973) estimated equilibrium temperatures of the Higashi-akaishi ultramafic rocks from the Gongen area to be 500–600 °C and emphasized that the Higashi-akaishi rocks were formed under the lowest temperature among the Alpine-type ultramafic rocks. This paper describes the petrological and mineralogical characteristics of GUM rocks from the Gongen area. Focusing on the element zoning patterns in orthopyroxene, a more complete history of the prograde *P–T* evolution is revealed than has been documented before.

GEOLOGICAL SETTING AND PETROGRAPHY

The Sanbagawa high *P/T* metamorphic belt represents the deepest exposed parts of the Mesozoic accretionary complexes in the Japanese Island arc and stretches throughout the Outer Zone (the Pacific Ocean side) of the South-west Japan for a length of roughly 800 km (Fig. 1). It mainly consists of meta-sedimentary and meta-volcanic rocks which originated in oceanic environments and subsequently suffered metamorphism related to Cretaceous subduction. There is no evidence for the collision of microcontinents or island arcs during its evolution. To the north the Sanbagawa belt is bounded by the Ryoke belt, which is characterized by low *P/T* metamorphism. Together these form perhaps the best known example of paired metamorphic belts (Miyashiro, 1961). The boundary between the Sanbagawa and Ryoke belts is a major strike-slip fault, the Median Tectonic Line (MTL).

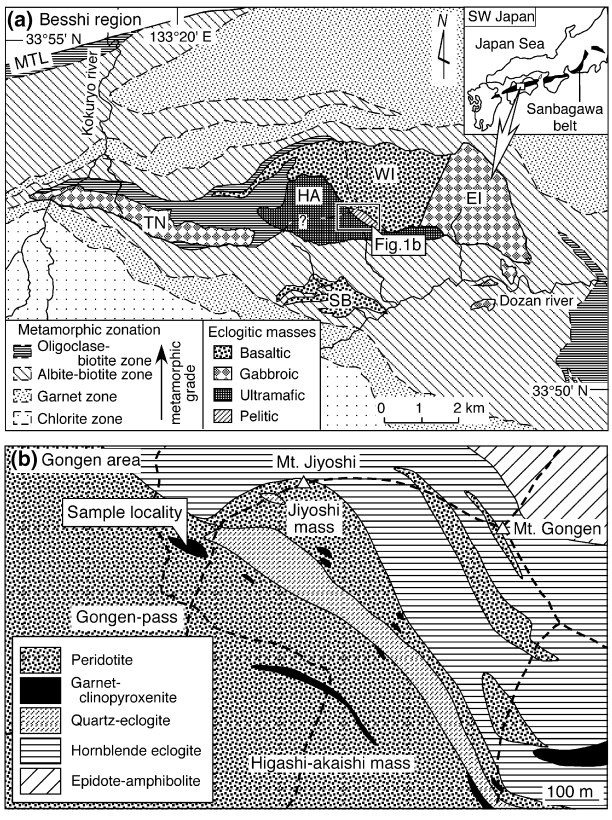

Fig. 1. Geological sketch maps of the (a) Besshi region (partly modified from fig. 1 of Aoya, 2001) and (b) Gongen area (simplified from fig. 4 of Kugimiya & Takasu, 2002). Abbreviations are: HA, Higashi-akaishi mass; TN, Tonaru mass; WI, Western Iratsu mass; EI, Eastern Iratsu mass; SB, Seba mass.

The Sanbagawa belt is divided into the chlorite, garnet, albite–biotite and oligoclase–biotite zones based upon mineral parageneses of pelitic schists in order of increasing metamorphic grade (Enami, 1983; Higashino, 1990). The high-grade albite–biotite and oligoclase–biotite zones are widely distributed in the Besshi region of central Shikoku (Fig. 1a). The metamorphic grade of these mineral zones is equivalent to that of the epidote-amphibolite facies, and *P–T* conditions have been estimated to be 0.7–1.0 Gpa and 480–620 °C (Enami *et al.*, 1994; Wallis *et al.*, 2000). Within the region of epidote–amphibolite facies metamorphism there are numerous ultramafic and mafic masses, such as the Higashi-akaishi and Jiyoshi peridotite masses, and then Iratsu, Tonaru and Sebadani metabasite masses which have protoliths of gabbro and basalt (Fig. 1: Kunugiza *et al.*, 1986). The Higashi-akaishi and Jiyoshi masses probably share the same petrogenesis and *P–T* evolution, although they are now separated by a kyanite quartz eclogite unit (Fig. 1b). The Besshi region is the only region in the Sanbagawa belt where a complex of high-grade mafic and ultramafic units are recognized. No GUM rocks are reported from other regions of the Sanbagawa belt. The mafic-ultramafic complex in the Besshi region underwent extensive recrystallization under epidote-amphibolite facies conditions; however, they also locally preserve evidence of a prior stage of eclogite facies metamorphism (e.g. Takasu, 1989; Wallis & Aoya, 2000).

The Higashi-akaishi mass is the largest ultramafic lens (5×1.5 km) in the Sanbagawa belt. Dunite, wehrlite and garnet clinopyroxenite are the dominant rock-types in this mass. Compositional layering is developed in the dunite and other rock-types. The Higashi-akaishi mass is thought to have formed as a cumulate under garnet-stable conditions of $P > 1.8$ GPa, and re-equilibrated under subsolidus conditions in the garnet–lherzolite facies and subsequently in the epidote–amphibolite facies (Kunugiza *et al.*, 1986). Dunite is the main constituent rock-type composed of olivine and Cr-spinel with subordinate amounts of serpentine, chlorite and magnetite. Chromitite layers up to 1 m thick are intercalated in the dunite and locally intensely folded (Mori & Banno, 1973). Olivine of the Higashi-akaishi mass is generally fine-grained (< 1 mm in size) and anhedral. It shows a wide variation in Mg# [$= Mg/(Mg + Fe^{2+})$] ranging from 0.83 to 0.97. A high Mg# (> 0.93) represents re-equilibration with Cr-spinel and other mafic phases under subsolidus conditions (Kunugiza, 1984). Cr-spinel is divided into retrograde- and igneous-types (Kunugiza, 1981). The retrograde-type Cr-spinel always coexists with serpentine and chlorite, and is strongly zoned with an Al-rich core and Fe^{3+}-rich rim which formed by a hydration reaction involving Cr-spinel and olivine. The igneous-type Cr-spinel shows a weak zoning with decreasing Cr and increasing Fe^{3+} towards the crystal rim, and does not coexist with any hydrous minerals. Cr-spinel including the retrograde-rim has a wide compositional range with Y_{Cr} [$Cr/(Cr + Al + Fe^{3+})$] value of 0.1–0.85 and TiO_2 content up to 3 wt%. Clinopyroxene has a variable Mg# from 0.76 to 0.97, with high Mg# compositions over 0.94 indicating relatively low temperature re-equilibration in the epidote-amphibolite facies or later stages (Kunugiza, 1984).

The Jiyoshi mass is an elongated and lenticular mass 150×800 m in size (Fig. 1b) mainly composed of wehrlite, harzburgite and clinopyroxenite (Mori & Banno, 1973; Kunugiza, 1984). Olivine and clinopyroxene contain magnetite, antigorite, tremolite and calcite as inclusions, and commonly have high Mg#s (0.89–0.94 for olivine, 0.94–0.96 for clinopyroxene and 0.93–0.94 for orthopyroxene). These facts suggest that the Jiyoshi mass is derived from serpentinized ultramafic rocks that underwent dehydration reactions during the final stage of prograde epidote-amphibolite facies metamorphism (Kunugiza, 1984). Typically the metamorphic assemblage is olivine + diopside + tremolite + antigorite for calcic ultramafic rocks. Some antigorite crystals replace olivine and are clearly

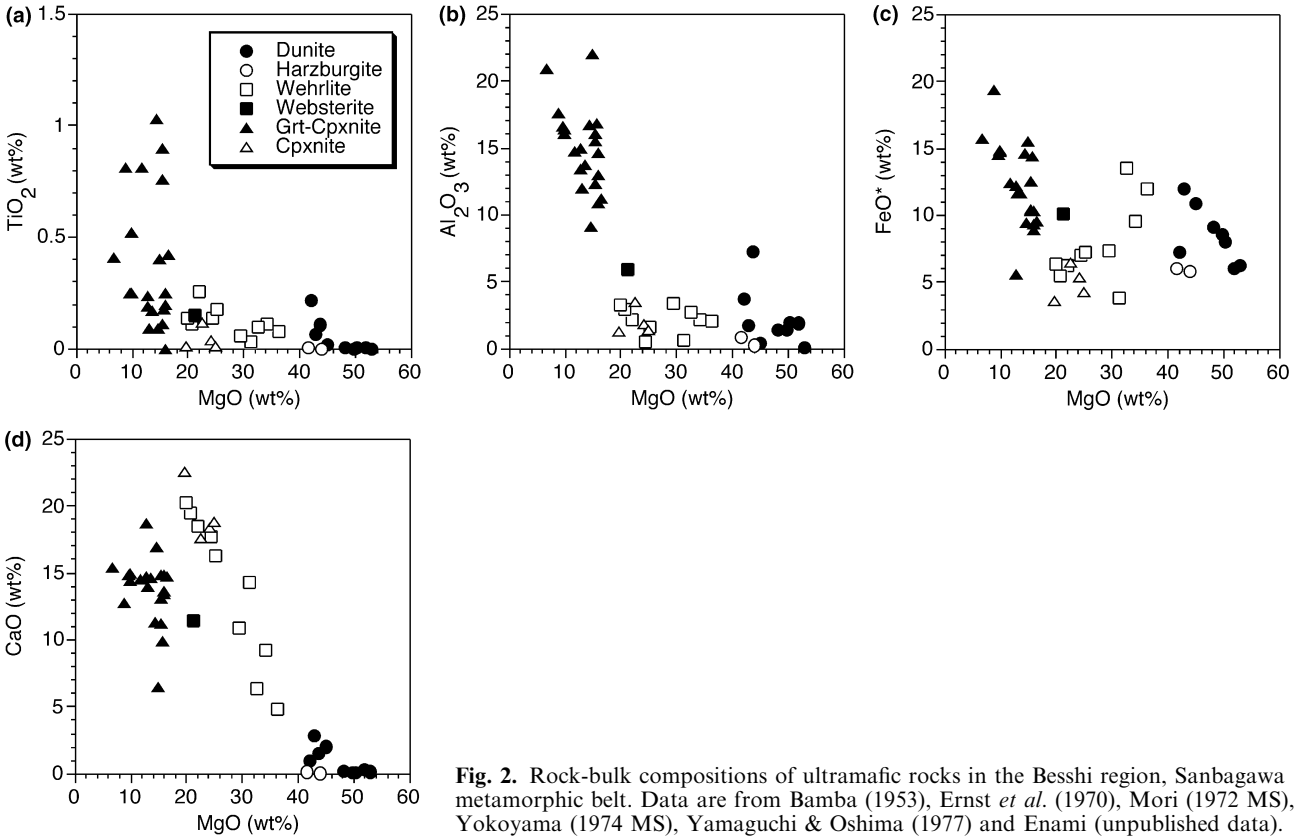

Fig. 2. Rock-bulk compositions of ultramafic rocks in the Besshi region, Sanbagawa metamorphic belt. Data are from Bamba (1953), Ernst *et al.* (1970), Mori (1972 MS), Yokoyama (1974 MS), Yamaguchi & Oshima (1977) and Enami (unpublished data).

retrograde products formed after the peak of the epidote-amphibolite facies metamorphism.

Bulk-rock compositions of ultramafic rocks in the Higashi-akaishi and Jiyoshi masses show systematic increases of TiO_2, Al_2O_3, total FeO and CaO with decreasing MgO in the order dunite, harzburgite, wehrlite, websterite and garnet–clinopyroxenite (Fig. 2). The layered structure and the wide and systematic variation of bulk-rock compositions imply that both ultramafic masses originally formed as a part of a cumulate sequence (e.g. Mori & Banno, 1973).

The samples used in the present study were all collected from the main cliff of the Gongen valley, north-west of the Gongen pass (Fig. 1b). In the Gongen valley, peridotites of the Higashi-akaishi and Jiyoshi masses are strongly sheared and mylonitized, resulting in the formation of a strong foliation (Fig. 3a). Wehrlite, garnet clinopyroxenite and websterite are relatively abundant in the Gongen valley. Coexisting orthopyroxene and garnet have been reported only from the Gongen outcrop in the Sanbagawa belt. Wehrlite grades into dunite, and contains subordinate amounts of ilmenite, magnetite and tremolite. Olivine and clinopyroxene are fractured and serpentinized/chloritized to various degrees. Large clinopyroxene crystals in the wehrlite contain exsolution lamellae of garnet, spinel and orthopyroxene, and are commonly surrounded by fine-grained and lamella-free clinopyroxene (Yokoyama, 1975). Garnet clinopyroxenite and websterite occur in mylonitized dunite as boudins with thicknesses from a few centimetres to 1 metre (Fig. 3b). Garnet clinopyroxenite is essentially bimineralic, but also contains minor amounts of ilmenite, rutile and Cr-rich magnetite. All constituent minerals have a similar grain size and are anhedral. Hornblende, tremolite and chlorite locally replace anhydrous minerals or occur along cracks. Websterite occurs as layers intercalated with garnet clinopyroxenite, and is mainly composed of orthopyroxene, garnet, clinopyroxene, magnetite and ilmenite. Recrystallization under epidote–amphibolite facies stage caused some mineralogical modifications in the Higashi-akaishi peridotites (Kunugiza, 1981, 1984).

SAMPLE DESCRIPTIONS

The garnet- and orthopyroxene-bearing ultramafic rocks investigated here are garnet clinopyroxenite (GO17O02b & H02), garnet websterite (GO02KY, GO03aKY & HA02) and garnet wehrlite (HBG01). Mineral assemblages are listed in Table 1. None of the studied samples show any significant development of kelyphitic or symplectitic coronas around garnet and pyroxene, respectively. The garnet wehrlite (HBG01) is distinct from the other five samples both in its appearance and mineral chemistry as will be described later. The garnet wehrlite occurs as a block in the debris and is petrologically more similar to ultramafic rocks in the Jiyoshi mass than those in the Higashi-akaishi mass.

GO17O02b (garnet clinopyroxenite)

A deformed zone of 0.5–1 cm in width containing garnet and orthopyroxene (CTC zone) separates a garnet clinopyroxenite boudin and the host dunite (Fig. 4a). The dunite is composed of olivine and Cr-spinel with minor garnet, and is strongly serpentinized. The bimineralic core of the garnet clinopyroxenite boudin contains subordinate amounts of ilmenite, pyrrhotite, pentlandite and retrograde chlorite. The deformed zone is subdivided into a clinopyroxene-poor (Cpp) part adjacent to the dunite and a clinopyroxene-rich (Cpr) part near to bimineralic core. The Cpp part is composed of olivine, orthopyroxene, garnet, clinopyroxene and Cr-spinel with retrograde edenite/pargasite and serpentine. The Cpr part consists of clinopyroxene, garnet, olivine, orthopyroxene, ilmenite, Cr-spinel, pyrrhotite and pentlandite with retrograde chlorite, serpentine and edenite/pargasite. Some garnet grains have rare inclusions of clinopyroxene, olivine, ilmenite and pentlandite. A garnet crystal contains fine-grained ($< 5\ \mu m$ in size) chlorite (Fig. 4b). There is no textural evidence for such chlorite replacing

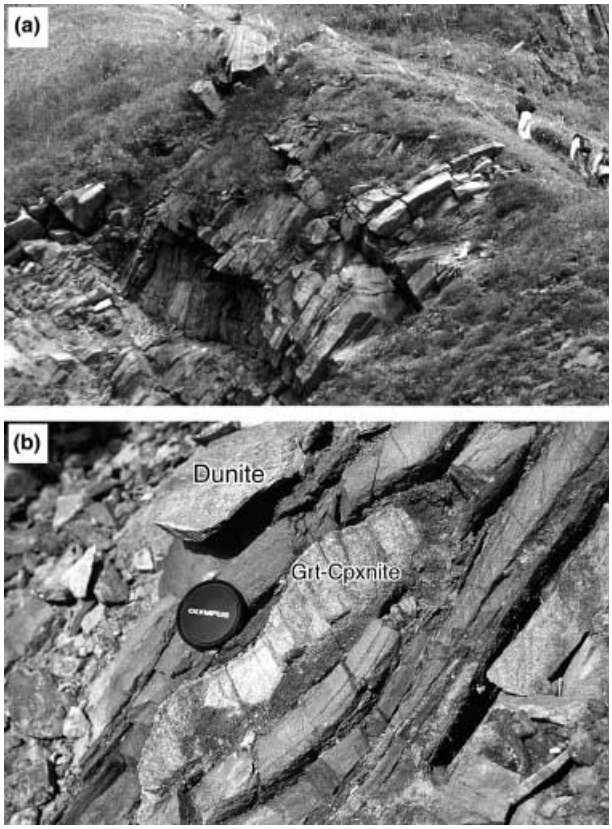

Fig. 3. Photographs showing (a) outcrop of sheared dunites of the Higashi-akaishi mass at Gongen area and (b) mode of occurrence of garnet clinopyroxenite lens in the sheared dunite.

garnet, implying that chlorite may have been stable during an early stage of prograde metamorphism. Rare fine-grained (100–300 μm in size) garnet is included in clinopyroxene. Magnetite partly rims ilmenite and is possibly a retrograde phase.

H02 (garnet clinopyroxenite)

This sample contains a boudinaged layer of garnet clinopyroxenite in a host serpentinized dunite (see fig. 5a of Tsujimori *et al.*, 2000), and shows petrographical characteristics similar to the sample GO17O02b. The boundary between the garnet clinopyroxenite and dunite is strongly deformed in a 1–2 cm thick band. Most of the deformed part is composed of serpentinized olivine and Cr-spinel. Orthopyroxene coexisting with garnet occurs in a thin zone (2–3 mm thick) adjacent to the garnet clinopyroxenite. This zone is composed of orthopyroxene, olivine, garnet and clinopyroxene with accessory pargasite, ilmenite and pentlandite. The silicate minerals other than pargasite are angular and anhedral, and their grain size varies from 50 to 300 μm. Pargasite occurs as 200–800 μm long prismatic crystals. This phase is unstable at peak pressure conditions (> 2.4–3.0 GPa: Liu *et al.*, 1996; Niida & Green, 1999). The pargasite is possibly a retrograde product formed during exhumation, although there is no direct textural evidence supporting this interpretation.

GO02KY (websterite)

The sample GO02KY is composed of alternating almost monomineralic layers of orthopyroxene, clinopyroxene and garnet (each 0.5–2 cm wide). The orthopyroxene-rich and clinopyroxene-rich layers contain small amounts of clinopyroxene and garnet, respectively, and orthopyroxene, clinopyroxene and garnet coexist in thin transitional zones 3–4 mm wide between the two layers (Fig. 5a). The garnet rich-layer includes clinopyroxene, orthopyroxene and retrograde chlorite. Ilmenite and pyrrhotite occur as accessory minerals in all three layers. Detailed chemical analyses were done mainly on a three phase-bearing zone between the orthopyroxene- and clinopyroxene-rich layers. Orthopyroxene and clinopyroxene occur as rounded and subhedral crystals, and reach 2.5 mm in size. Large crystals of orthopyroxene contain rare clinopyroxene, hornblende/edenite and magnetite as inclusions (1–10 μm in size: Fig. 4c). The pyroxene are partly rimmed by retrograde tremolite. Garnet is anhedral (100–500 μm in size) and commonly occurs at grain boundaries between pyroxene crystals. Polycrystalline aggregates of garnet rarely enclose small crystals of orthopyroxene and clinopyroxene (20–50 μm in size).

HA02 and GO03aKY (websterite)

These samples show alternations of clinopyroxene-rich layers (2–5 cm in width) and monomineralic layers of garnet or orthopyroxene (0.5–1.5 cm in width): a photograph of the polished sample HA02 is shown in fig. 5(b) of Tsujimori *et al.* (2000). The clinopyroxene-rich layer on which chemical analyses have been done is composed of clinopyroxene, orthopyroxene and garnet with minor ilmenite, pyrrhotite and magnetite. This layer shows a compositional heterogeneity with alternations of thin orthopyroxene-rich and garnet-rich parts 0.5–1 cm in width (Fig. 5b). Modal amounts of clinopyroxene in the clinopyroxene-rich layers are 60–80% in HA02 and 40–60% in GO03aKY. Clinopyroxene and orthopyroxene occur as rounded and anhedral grains 0.1–1 mm in diameter. In GO03aKY, fine-grained clinopyroxene crystals (< 20 μm) are included in orthopyroxene. Garnet (100–300 μm in size) is more anhedral and angular than pyroxene and commonly occurs as an interstitial phase between pyroxene crystals. However, fine-grained garnet is included in pyroxene, thus garnet was possibly stable during the pyroxene re-crystallization. Retrograde tremolite and chlorite locally rim pyroxene and garnet.

Table 1. Mineral assemblages of garnet-bearing ultramafic rocks from the Gongen arean, Sanbagawa belt.

Sample No.	Rock-types	Layer	Grt	Opx	Cpx	Ol	Amp	Chl	Mag	Ilm	Others
GO17O02b	Grt-cpxnite	Cpp	+	+	+	+	r				Cr-Spl, (Srp)
		Cpr	+	+	+	+	r	i, r	r	+	Cr-Spl, Po, Pn, (Srp)
H02	Grt-cpxnite		+	+	+	+	r			+	Pn, (Srp)
GO02KY	websterite		+	+	+		i, r	r	+, i	+	Po
HA02	websterite		+	+	+		r	r	+	+	Po
GO03aKY	websterite		+	+	+		r	r	+	+	Po
HBG01	wehrlite		+	+	+	+		r	+, i	i	Po, Pn, (Srp)

Abbreviations: Cpp, clinopyroxene-poor layer; Cpr, clinopyroxene-rich layer; +, primary phase at peak metamorphic stage; s and mineral in parenthesis, retrograde phase after peak metamorphic stage; i, early stage phase included in garnet or pyroxene; Grt, garnet; Opx, orthopyroxene; Cpx, clinopyroxene; Ol, olivine; Amp, amphibole; Chl, chlorite; Mag, magnetite; Ilm, ilmenite; Cr-Spl, Cr-rich spinel; Srp, serpentine; Po, pyrrhotite; Pn, pentlandite.

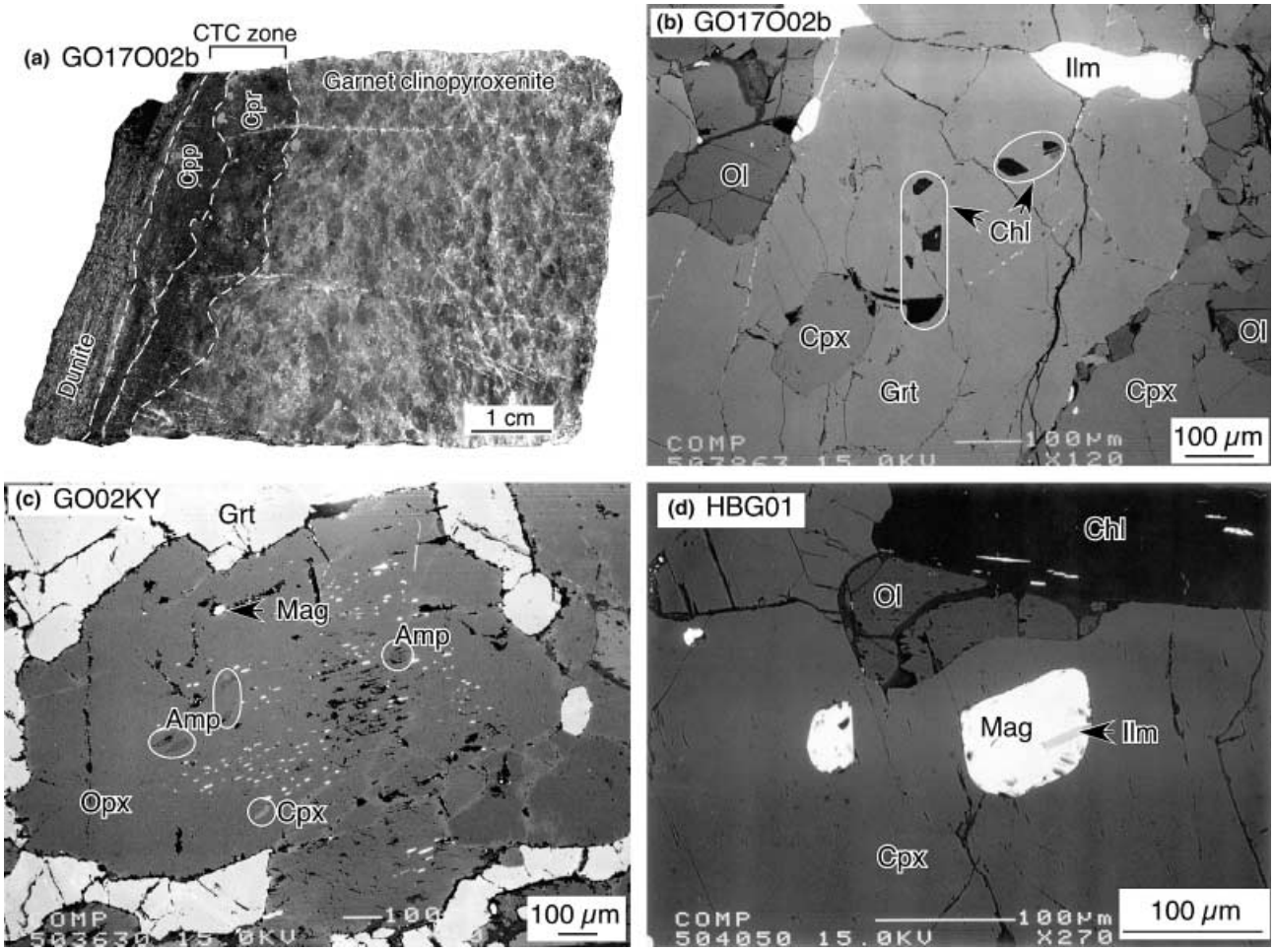

Fig. 4. Photograph of polished surface of sample GO17O02b (a) and back-scattered electron images of samples GO17O02b (b), GO02KY (c) and HBG01 (d). Abbreviations are defined in Table 1 and text.

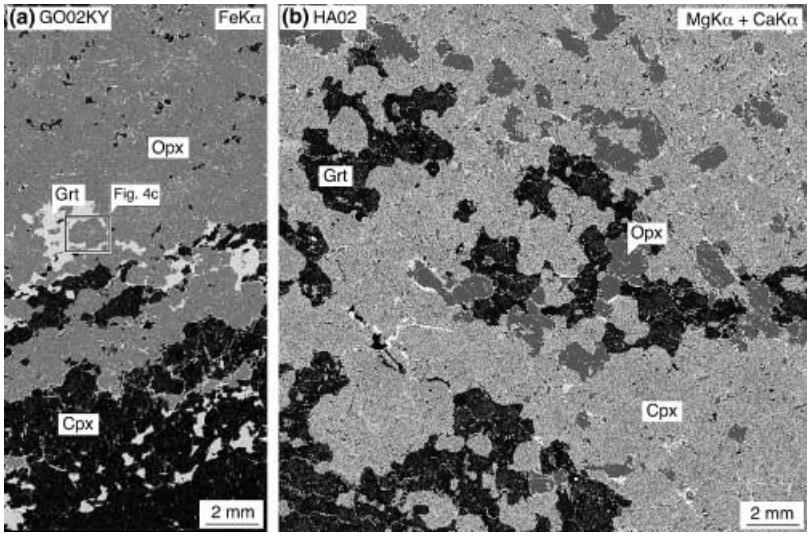

Fig. 5. X-ray mapping images of (a) GO02KY for FeKα and (b) GO03aKY for MgKα and CaKα. Lighter parts indicate higher concentration of elements.

HBG01 (wehrlite)

The sample is foliated and composed of alternating thin (2–5 mm wide) olivine-rich and clinopyroxene-rich layers. The olivine-rich layers include subordinate amounts of orthopyroxene and clinopyroxene and commonly lack garnet. The clinopyroxene-rich layer contains garnet and subordinate amounts of orthopyroxene and olivine. The silicate minerals are anhedral and locally fractured. Magnetite, pentlandite and pyrrhotite occur both as inclusions in silicate minerals and a discrete grains in the matrix. Ilmenite occurs as inclusions forming composite grains with magnetite in silicate minerals (Fig. 4d). Garnet is 0.5–2 mm in size, and rarely contains inclusions of other constituent silicate minerals. Orthopyroxene occurs as rounded and spindle-shaped crystals with a maximum length of 0.5 mm partly rimmed by serpentine. Clinopyroxene shows a grain-shape similar to orthopyroxene and its grain size reaches 1.5 mm in length. Olivine is strongly replaced by serpentine both along cracks and around its rim.

MINERAL CHEMISTRY

Chemical compositions of minerals were analyzed using a JEOL JXA-8800R (WDS + EDS) electron-probe microanalyzer at Nagoya University. Accelerating voltage, specimen current and beam diameter for quantitative analyses were 15 kV, 12 nA on the Faraday cup and 2–3 μm, respectively. Well-characterized natural and synthetic silicate and oxide standards were used for calibration. The ZAF method was employed for matrix correction. Estimates of errors for Al_2O_3 and Cr_2O_3 contents of pyroxene are 4–5% and 10–12% (2 σ level), respectively. All Fe in garnet and pyroxene was assumed to be ferrous because (1) Fe_2O_3 contents in ultramafic rocks are generally considered to be negligible (e.g. Krogh & Carswell, 1995) and (2) all samples other than H02 contain pyrrhotite implying low oxygen fugacity during metamorphism (e.g. Itaya *et al.*, 1985). Amphibole formulae are described using an average of the maximum and minimum Fe^{3+} contents suggested by Leake *et al.* (1997). The ferric to ferrous ratio of oxide minerals is estimated assuming an ideal formula

Table 2 Compositional ranges of major constituent minerals of garnet-bearing ultramafic rocks from the Gongen area, Sanbagawa belt.

Sample No.	Rock-types	Layer	Note	Nbp						
Garnet					Xalm	Xprp	Xgrs	Xsps	Cr_2O_3*	Mg#
GO17O02b	Dunite		Mrx	12	0.22–0.26	0.58–0.62	0.15–0.16	0.01–0.02	0.71–1.30	0.69–0.74
	Grt-cpxnite	Cpp	Mrx	74	0.24–0.28	0.55–0.60	0.13–0.16	0.01–0.02	0.27–1.41	0.66–0.72
		Cpr	Mrx	179	0.27–0.33	0.51–0.57	0.14–0.18	0.00–0.01	0.10–1.39	0.61–0.68
		Bmc	Mrx	144	0.27–0.32	0.52–0.57	0.15–0.19	0.00–0.01	0.04–0.43	0.62–0.68
H02	Grt-cpxnite		Mrx	44	0.23–0.30	0.55–0.61	0.13–0.15	0.01–0.02	0.69–1.22	0.65–0.73
GO02KY	websterite		Mrx	117	0.37–0.46	0.34–0.47	0.14–0.18	0.00–0.02	0.22–0.84	0.43–0.56
HA02	websterite		Mrx	46	0.32–0.36	0.48–0.53	0.13–0.15	0.01–0.02	0.24–0.47	0.57–0.63
GO03aKY	websterite		Mrx	43	0.38–0.44	0.39–0.47	0.14–0.19	0.01–0.02	0.46–1.15	0.47–0.56
HBG01	wehrlite		Mrx	220	0.28–0.32	0.48–0.55	0.15–0.19	0.02–0.03	0.09–0.40	0.60–0.67
Orthopyroxene					Al_2O_3*	CaO*			Cr_2O_3*	Mg#
GO17O02b	Grt-cpxnite	Cpp	Mrx	111	0.27–0.81	0.06–0.40			0.01–0.13	0.88–0.90
		Cpr	Mrx	190	0.33–1.13	0.10–0.36			0.01–0.13	0.86–0.88
H02	Grt-cpxnite		Mrx	83	0.44–2.63	0.07–0.29			0.04–0.15	0.88–0.90
GO02KY	websterite		Mrx	60	0.35–1.17	0.11–0.32			0.01–0.15	0.80–0.82
			InG	13	0.61–0.79	0.23–0.29			0.03–0.09	0.80–0.82
HA02	websterite		Mrx	137	0.45–1.09	0.11–0.30			0.00–0.10	0.82–0.85
GO03aKY	websterite		Mrx	117	0.32–2.07	0.12–0.32			0.01–0.16	0.79–0.83
			InG	12	0.60–1.11	0.23–0.31			0.05–0.22	0.79–0.82
HBG01	wehrlite		Mrx	320	0.37–1.69	0.07–0.50			0.00–0.09	0.85–0.88
			InG	59	1.10–1.74	0.16–0.42			0.00–0.09	0.86–0.88
			InC	11	1.26–1.35	0.27–0.42			0.01–0.07	0.86
Clinopyroxene					Al_2O_3*		Na_2O*		Cr_2O_3*	Mg#
GO17O02b	Grt-cpxnite	Cpp	Mrx	55	0.56–0.95		0.34–0.47		0.05–0.29	0.93–0.95
		Cpr	Mrx	164	0.52–1.06		0.32–0.56		0.02–0.29	0.92–0.95
		Bmc	Mrx	114	0.55–1.06		0.30–0.49		0.00–0.12	0.91–0.95
H02	Grt-cpxnite		Mrx	57	0.61–1.05		0.28–0.46		0.15–0.32	0.93–0.94
GO02KY	websterite		Mrx	66	0.65–1.37		0.49–0.76		0.04–0.24	0.87–0.90
			InG	12	0.62–0.77		0.53–0.62		0.09–0.16	0.89–0.90
HA02	websterite		Mrx	67	0.55–0.90		0.32–0.51		0.02–0.15	0.90–0.92
GO03aKY	websterite		Mrx	34	0.73–1.20		0.49–0.81		0.07–0.33	0.87–0.90
			InG	11	0.74–1.09		0.56–0.73		0.11–0.30	0.89–0.91
HBG01	wehrlite		Mrx	201	0.33–1.45		0.06–0.18		0.00–0.08	0.90–0.93
			InG	10	0.52–0.84		0.09–0.11		0.02–0.07	0.91–0.93
Olivine								NiO*		Mg#
GO17O02b	Duniite		Mrx	30				0.14–0.24		0.90–0.91
	Grt-cpxnite	Cpp	Mrx	78				0.17–0.31		0.88–0.89
		Cpr	Mrx	55				0.10–0.25		0.85–0.88
H02	Grt-cpxnite		Mrx	7				0.17–0.27		0.89–0.90
HBG01	wehrlite		Mrx	34				0.07–0.14		0.87–0.88
Cr-spinel					Al_2O_3*				Cr_2O_3*	Mg#
GO17O02b	Dunite		Mrx	28	13.9–25.1				34.0-40.5	0.28–0.41
	Grt-cpxnite	Cpp	Mrx	16	12.9–16.6				34.7-40.2	0.24–0.31
		Cpr	Mrx	19	4.8–7.7				23.0-27.4	0.13–0.27

* wt%.

Abbreviations: Nbp, numbers of analytical points; Bmc, bimineralic core; Mrx, matrix phase; InG, inclusion phase in garnet; InC, inclusion phase in clinopyroxene. Others are defined in Table 1 and text.

and charge valance. Compositional ranges and representative analyses of the major constituent minerals of the GUM rocks studied are given in Tables 2 and S1, respectively. Abbreviations for minerals and molar components follow Kretz (1983) and Miyashiro (1994).

Garnet

Garnet is chemically homogeneous other than its rim where pyrope $\{X_{Prp} = Mg/(Fe + Mn + Mg + Ca)\}$ content slightly decreases and almandine content (X_{Alm}) shows the opposite trend (Fig. 6a). The amount of compositional change in Mg# between the core and outer-most rim parts [Mg# (core-rim)] is small, commonly < 0.03 (Table S1). Garnet zoning at the interfaces with clinopyroxene and olivine is more pronounced than that at the garnet–orthopyroxene interface (Fig. 6a). In the sample GO17O02b the Mg# (core-rim) of garnet rims in contact with olivine, clinopyroxene and orthopyroxene reach 0.07, 0.06 and 0.03, respectively. Similar patterns are observed in other samples. In sample HBG01, for example, a profile across a composite inclusion of orthopyroxene-clinopyroxene in garnet clearly shows that compositional modification of garnet is higher next to clinopyroxene than next to orthopyroxene (Fig. 6b).

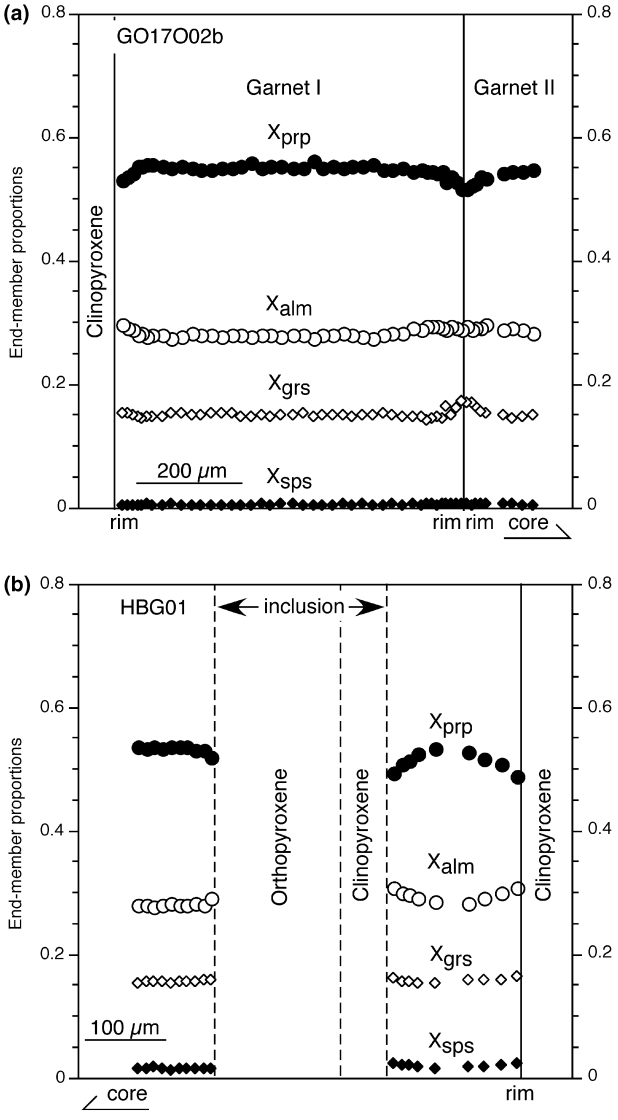

Fig. 6. Zoning profiles of garnet in samples (a) GO17O02 and (b) HBG01. The garnet in HBG01 has a composite inclusion of orthopyroxene and clinopyroxene.

Garnet belongs to the grossular-rich pyrope-almandine series (Tables 2 & S1). The Cr_2O_3 contents are variable and reach 1.4 wt% in garnet-clinopyroxenite. Garnet in the Cpp and Cpr parts of the sample GO17O02b have compositional ranges similar to those in the bounding dunite and garnet clinopyroxenite, respectively. This chemical characteristic implies that the Cpp and Cpr parts are deformed dunite and garnet clinopyroxenite, respectively. Pyrope content of garnet in the garnet-clinopyroxenite and wehrlite is slightly higher than that in the websterite.

Orthopyroxene

Three types of orthopyroxene can be defined with regard to Al zoning and texture. Most orthopyroxene crystals show distinct bell-shaped Al zoning with a continuous decrease of Al content from core to rim (Figs 7a & 8a). Some orthopyroxene crystals adjacent to garnet display W-shaped Al zoning profiles in which Al content slightly increases near their interface (Fig. 8b). Orthopyroxene included in garnet and clinopyroxene is compositionally homogeneous and does not show a distinct decrease of Al at the mantle part of crystals (Fig. 8c). The Mg# of the bell-shaped Al zoned orthopyroxene is fairly constant or decreases slightly at the interface with garnet and shows the opposite trend at the interface with clinopyroxene. Calcium in orthopyroxene increases slightly at the outer most rim in all samples with the exception of HBG01, where orthopyroxene shows the opposite trend. The increase of Ca at the rim is more pronounced adjacent to clinopyroxene.

In all the studied GUM samples studied, the matrix orthopyroxene has similar compositions, and the bell-shaped Al zoned orthopyroxene grains all have a similar Al_2O_3 content of 0.3–0.5 wt% at the crystal rim in all the rock types. The Al_2O_3 contents of orthopyroxene included in garnet and clinopyroxene are commonly more than 0.6–1.1 wt%, similar to those of the core parts of matrix orthopyroxene (Fig. 8c & Table 2). Fine-grained orthopyroxene surrounded by aggregates of polycrystalline garnet (sample GO02KY) also have an Al-richer composition than the rim part of matrix orthopyroxene. TiO_2 contents are < 0.1 wt%.

Clinopyroxene

Two types of zoning are recognized. The most common type is characterized by a continuous increase of Mg# and a decrease of Al from core to rim, similar to the bell-shaped zoning of orthopyroxene (Figs 7b & 9a). This type of zonal structure is observed in all the samples studied. Another type of U-shaped Al zoning, which occurs in the sample HBG01, is composed of a relatively homogeneous core that has an Al-poor composition and a mantle part that shows increasing Al content towards the rim (Fig. 9b). The Mg# of this clinopyroxene shows the opposite trend to the Al content. Clinopyroxene is an Al- and Na-poor diopside, and is similar in composition among in both the garnet clinopyroxenite and websterite samples. Clinopyroxene in the wehrlite sample HBG01 is slightly poorer in Cr and Na than other samples. TiO_2 content is < 0.11 wt%.

Olivine

Olivine in sample GO17O02b shows a systematic decrease of Mg# from the host dunite (0.90–0.91) through the Cpp part (0.88–0.89) to Cpr part (0.85–0.88). NiO is rather variable, but shows no compositional difference among the three parts (Table 2). Mg# is fairly constant in the other two samples (H02 and HBG01), and the NiO content shows a similar variation as in GO17O02b.

Amphibole

Amphibole included in orthopyroxene in sample GO02KY has an edenitic composition with $Al_2O_3 = 9.4–10.1$ wt%, $Na_2O =$

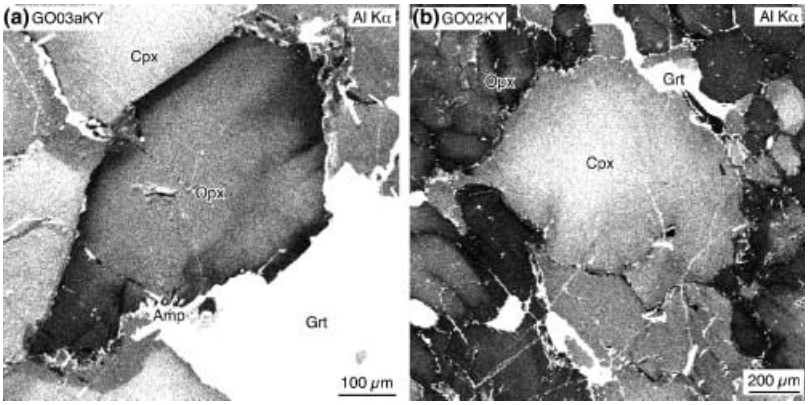

Fig. 7. AlKα X-ray mapping images of (a) orthopyroxene in GO03aKY and (b) clinopyroxene in GO02KY. Lighter parts indicate higher concentration of element.

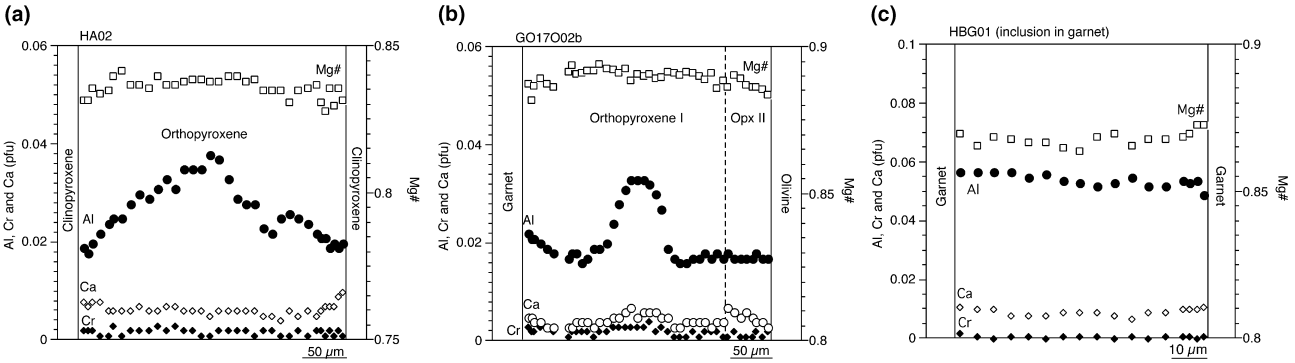

Fig. 8. Zoning profiles of orthopyroxene with (a) bell-shaped Al zoning (HA02) and (b) W-shaped Al zoning (GO17O02b) and (c) included in garnet (HBG01).

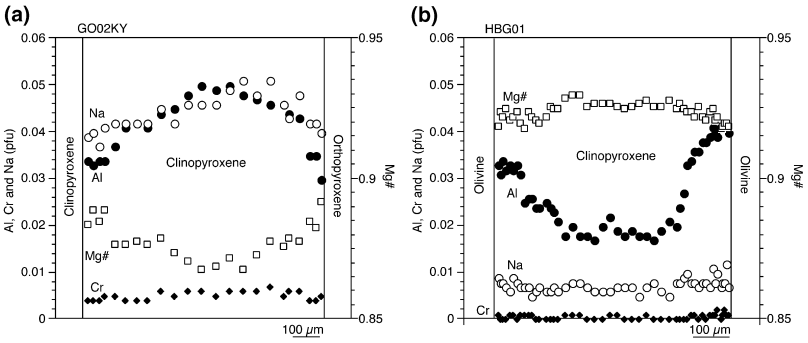

Fig. 9. Zoning profiles of clinopyroxene with (a) bell-shaped Al zoning and (b) U-shape Al zoning.

2.3–2.5 wt%, K_2O = 1.0–1.1 wt% and Mg# = 0.88–0.90. Retrograde amphibole in garnet clinopyroxenite (GO17O02b & H02) have similar Al_2O_3 (9.9–12.7 wt%) and Na_2O (1.8–2.8 wt%) contents to the inclusion amphibole. The corresponding K_2O contents and Mg#s lie in the ranges 0.5–3.6 wt% and 0.93–0.97, respectively. The Cr_2O_3 contents of amphibole in GO17O02b are variable from 0.8 to 1.3 wt% in the host dunite to 0.1–0.2 wt% in the Cpr part, and those of H02 range from 0.4 to 0.9 wt%. Retrograde amphibole replacing pyroxene and garnet in websterite and wehrlite are tremolite with Al_2O_3 = 0.3–1.7 wt%, Na_2O = 0.1–0.3 wt% and Mg# = 0.92–0.96.

Chlorite

Retrograde chlorite is clinochlore with Si = 2.95–3.06 per formula unit (pfu), Al = 2.00–2.20 pfu and Mg# = 0.89–0.94. In sample GO17O02b, chlorite included in garnet (Si = 3.02–3.25 pfu, Al = 1.91–2.08 pfu and Mg# = 0.94–0.95) is slightly more enriched in Cr_2O_3 (0.50–0.65 wt%) than the retrograde one (0.13–0.45 wt%).

Oxide minerals

Spinel group minerals in GO17O02b show a variation in composition from Cr-spinel in the host dunite and Cpp part to magnetite in the Cpr part. Cr-spinel in dunite shows a weak zoning in which Al_2O_3 content and Mg# increase and Cr_2O_3 content decreases from core to rim. The composition of Cr-spinel ranges from Al_2O_3 = 13.9–25.1 wt%, Cr_2O_3 = 34.0–40.5 wt% and Mg# = 0.28–0.41 in the dunite and Al_2O_3 = 4.8–7.7 wt%, Cr_2O_3 = 23.0–27.4 wt% and Mg# = 0.13–0.27 in the Cpr part (Table 2). Magnetite in the Cpr part of GO17O02b and in other samples contains small amounts of

Al_2O_3 (1.4–1.9 wt%), Cr_2O_3 (5.9–7.2 wt%) and MgO (Mg# = 0.04–0.06). Ilmenite contains MgO in the ranges 4.8–6.3 wt% in garnet clinopyroxenite, 3.0–3.6 wt% in websterite and 10.0–10.2 wt% in wehrlite.

EQUILIBRIUM CONDITIONS

Orthopyroxene–garnet system

The following chemical and textural evidence indicates that the Al-zoning of orthopyroxene was formed by a reaction including garnet: (1) compositional similarities between orthopyroxene inclusions in garnet and the Al-rich core of matrix orthopyroxene, and (2) formation of W-shaped Al zoning by local re-equilibrium of bell-shaped Al zoned orthopyroxene at the interface with garnet. Thus, the orthopyroxene–garnet thermobarometers are applied to estimate *P–T* conditions of the orthopyroxene-bearing GUM rocks (Fig. 10). Pressure is calculated from the Al-barometers of Harley & Green (1982), Harley (1984b), Nickel & Green (1985), Brey & Köhler, 1990) and Holland & Powell (1998). Temperature is determined using Mg-Fe exchange thermometers of Harley (1984a), Sen & Bhattacharya (1984) and Carswell & Harley (1990).

Models of Mg-tschermak [X_{Al}(ts)] component in orthopyroxene considerably affect the pressure estimation in high-pressure and/or low-temperature rocks especially for Al-poor orthopyroxene assemblage (e.g. Carswell & Harley, 1990; Carswell, 1991; Taylor, 1998). There are three models of the Mg-tschermak component for jadeite- and aegirine-negligible orthopyroxene: X_{Al}(ts) (1) = Al/2 (Harley & Green, 1982; Harley, 1984a), X_{Al}(ts) (2) = (Al-Cr-2Ti + Na)/2 (Nickel & Green, 1985; Brey & Köhler, 1990), and X_{Al}(ts) (3) = (Al-Cr + Ti + Na)/2 (Taylor, 1998). The orthopyroxene studied commonly has low Ti and Cr contents up to 0.002 and 0.003 pfu, respectively, and Na content is commonly below the detection limit of 0.001 pfu. Thus difference in the X_{Al} (ts) values estimated by models (1) and (2) and models (1) and (3) are up to 10 and 5% of X_{Al} (ts) (1), respectively, and the difference can result in a maximum variation of 0.15 GPa in the estimated pressure. Among the four geobarometers, calibrations of Brey & Köhler (1990) and Harley (1984a) yield the highest and lowest pressure conditions, respectively (Fig. 10a). The difference between the two estimates ranges from 0.2 to 1.2 GPa with increasing X_{Al} (ts) of orthopyroxene. Variation of temperatures estimated by employing the three garnet–orthopyroxene thermometers is 30–60 °C.

The *P–T* conditions are estimated at 1.5–2.4 GPa/700–800 °C for cores and 2.9–3.8 GPa/700–810 °C for the rim of the bell-shaped Al zoned orthopyroxene for all samples. The *P–T* conditions estimated by using the composition of inclusions of orthopyroxene and their host garnet are 1.3–2.4 GPa/670–770 °C, and are similar to the result for the core of the bell-shape Al-zoned crystals (Fig. 10c,d,f). When pairs of the rim of the W-shaped zoned orthopyroxene and adjacent garnet are used, slightly lower *P–T* conditions of 1.8–3.0 GPa/630–780 °C than those for the bell-shaped Al-zoned orthopyroxene are derived (Fig. 10a,c,f).

Clinopyroxene- or olivine-bearing systems

Two-pyroxene thermometers (Bertrand & Mercier, 1985; Brey & Köhler, 1990; Taylor, 1998), the garnet–olivine thermometer (O'Neill & Wood, 1979, 1980), clinopyroxene–garnet Cr thermobarometry (Nimis & Taylor, 2000) and garnet–clinopyroxene Mg–Fe thermometer (Ai, 1994; Berman *et al*., 1995; Krogh Ravna, 2000) can be applied to clinopyroxene and olivine bearing samples. On average the two-pyroxene thermometers give 720–770 °C using core compositions and 680–790 °C using rim compositions for a nominal pressure of 3 GPa. Applying this thermometer to orthopyroxene inclusions and host clinopyroxene gives an average *T* of 710 °C at a pressure of 3 GPa (Fig. 10f). The garnet–olivine thermometer gives slightly lower and more limited temperature ranges of 645–680 °C (at *P* = 3 GPa) than the garnet–orthopyroxene and two-pyroxene thermometers. Clinopyroxene–garnet Cr thermobarometry proposed by Nimis & Taylor (2000) was applied using 219 spot data of clinopyroxene coexisting with garnet, orthopyroxene and olivine in the Cpp and Cpr parts of GO17O02b for the highest Cr compositions among the samples studied (Fig. 11). The *P–T* conditions estimated by clinopyroxene compositions have a peak frequency at 3–4 GPa and 700–850 °C, respectively. Increasing pressure and *P/T*-values during clinopyroxene re-crystallization are also recorded in a zoned clinopyroxene (Fig. 12). On average, garnet-clinopyroxene Mg-Fe thermometers give 650–720 °C for core compositions and 595–650 °C for rim compositions at *P* = 3 GPa. The low temperature estimates given by the garnet-clinopyroxene thermometer is possibly due to (1) Mg–Fe re-equilibration between these two phases continuing to take place after the peak of temperature (Fig. 6b) and/or (2) Mg–Fe diffusions rates in clinopyroxene and garnet being larger than those of other elements.

P–T trajectory

The *P–T* trajectory can be deduced from the mineral zoning patterns and the *P–T* estimates discussed above (Fig. 13). The following common characteristics are observed in all the GUM rocks: (1) lower temperature equilibrium of the Gongen GUM rocks than is typical of similar rock types in other orogenic belts (e.g. Brueckner & Medaris, 2000) (2) increase of pressure and *P/T* during the prograde evolution, and (3) little compositional re-equilibrium after peak *P–T* conditions. Information about an early stage of low-*P*

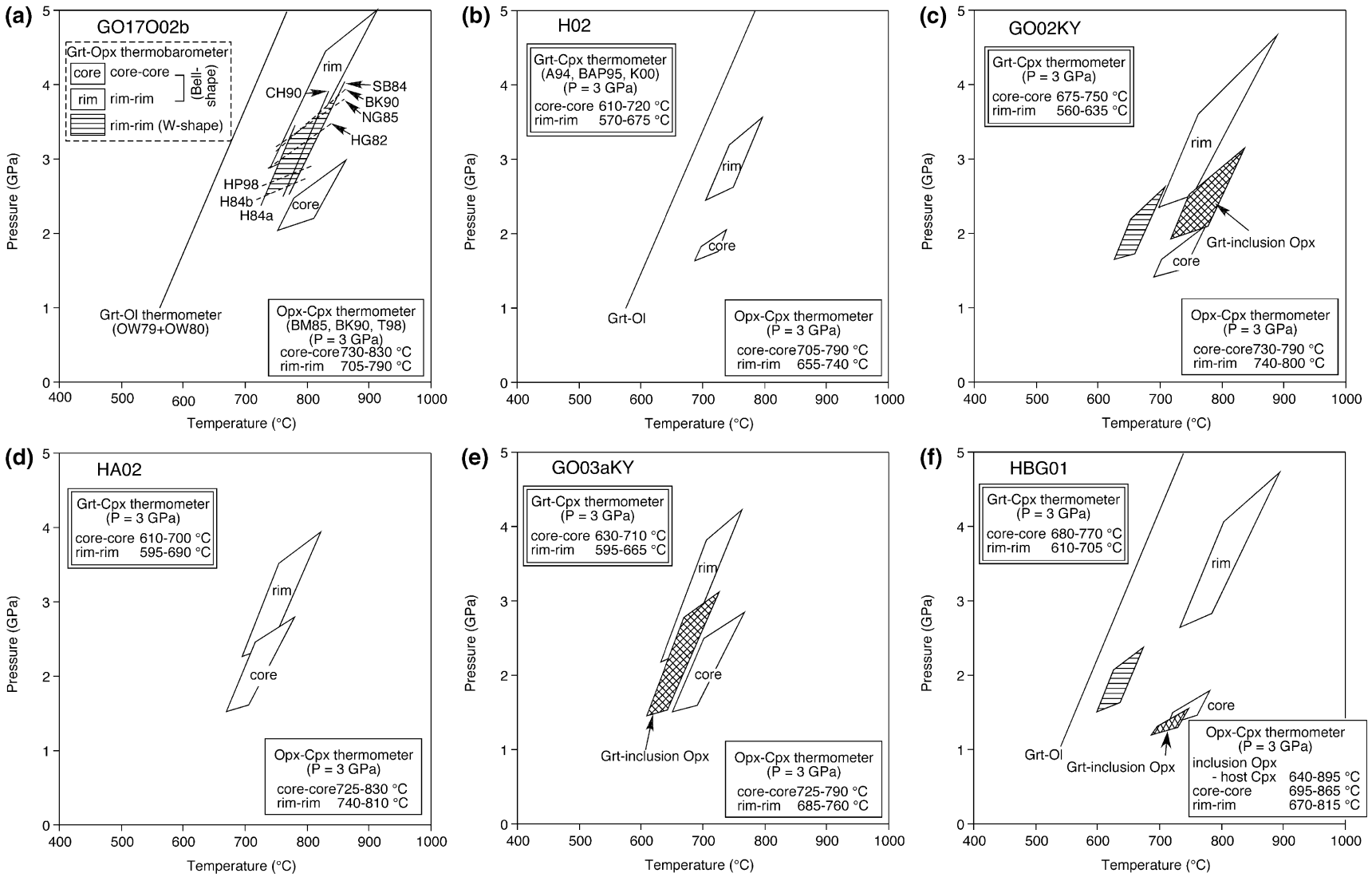

Fig. 10. Thermobarometric calculations and inferred *P–T* evolution of six GUM rocks from the Gongen area. Abbreviations for thermobarometers are: H84a (Harley, 1984a); SB84 (Sen & Bhattacharya, 1984); CH90 (Carswell & Harley, 1990); HG82 (Harley & Green, 1982); H84b (Harley, 1984b); NG85 (Nickel & Green, 1985); BK90 (Brey & Köhler, 1990); HP98 (THERMOCALC Ver. 3.1 and AX 2.2: Holland & Powell, 1998); BM85 (Bertrand & Mercier, 1985); Taylor (1998); OW79 (O'Neill & Wood, 1979); OW80 (O'Neill & Wood, 1980); A94 (Ai, 1994); BAP95 (Berman *et al.*, 1995), K00 (Krogh Ravna, 2000).

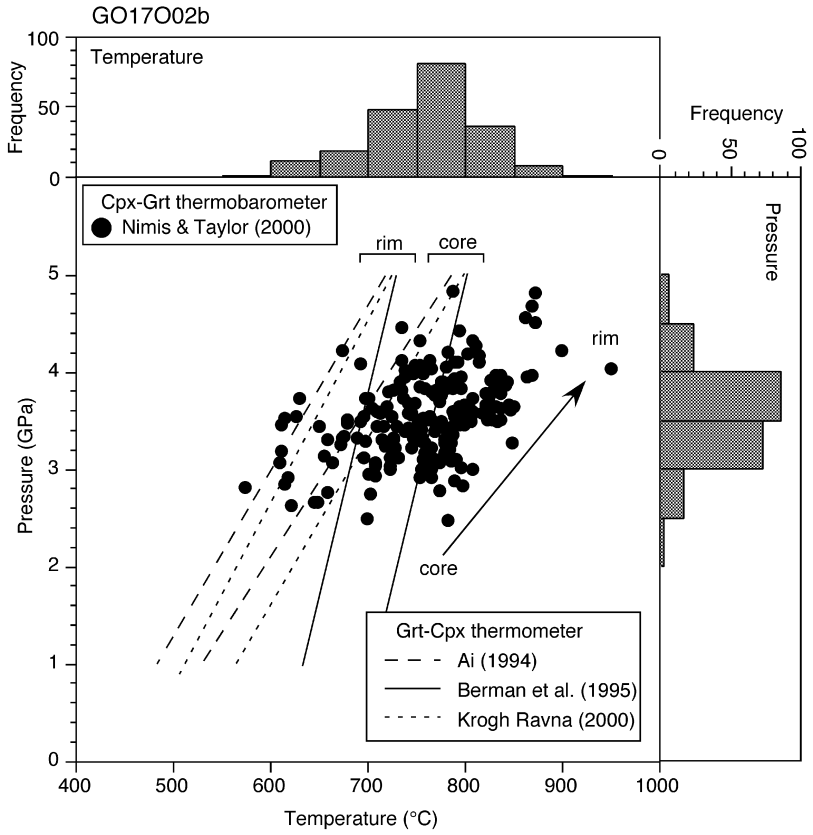

Fig. 11. Thermobarometric calculations of garnet-clinopyroxene assemblage of sample GO17O02b.

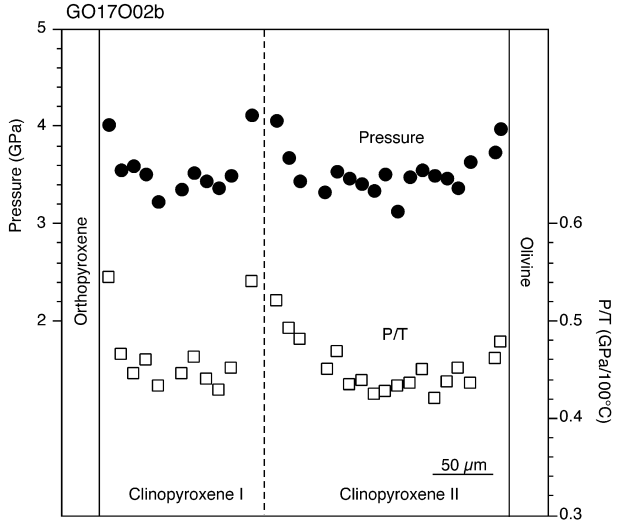

Fig. 12. Pressure and *P/T* evolution from a zoned clinopyroxene in sample GO17O02b using clinopyroxene-garnet Cr thermobarometer (Nimis & Taylor, 2000).

equilibrium during prograde metamorphism is preserved in the cores of minerals and as inclusions of hydrous phases. The estimated *P–T* conditions using core compositions of orthopyroxene are as low as 700–800 °C and 1.5–2.4 GPa. The existence of Mg-chlorite and edenitic amphibole as inclusions in orthopyroxene (samples GO17O02b & GO02KY) limits the upper temperature conditions to 800–900 °C for the growth stage of orthopyroxene core. Experimental data on amphibole stability and chemistries in various ultramafic bulk rock compositions show that Al and Na contents of amphibole systematically increase with increasing *P–T* conditions and have little dependence on bulk composition (Mengel & Green, 1989; Wallace & Green, 1991; Ernst & Liu, 1998; Niida & Green, 1999). Aluminium isopleths (Ernst & Liu, 1998) yield pressure conditions of 1.0 GPa at 600 °C and 0.8 GPa at 700 °C for an early stage of prograde metamorphism based on the compositions of amphibole included in orthopyroxene in the sample GO02KY (Table S1). These facts suggest that the Gongen GUM rocks have experienced amphibole granulite or lower *T* facies metamorphism at an early stage of prograde metamorphism. In addition orthopyroxene and olivine in sample HBG01 include fine-grained magnetite possibly indicating serpentinization before the re-crystallization of major phases as discussed by Kunugiza (1980). Thus this sample might have suffered metamorphism under lower *T* and/or higher H_2O-fugacity conditions than the other five samples.

The chemical equilibria at peak *P–T* conditions are commonly preserved at rims of minerals, including bell-shaped Al zoned orthopyroxene. Pressure conditions of the peak stage range from 2.9 to 3.8 GPa and are distinctly higher than the early stage of orthopyroxene formation. Temperature conditions for the

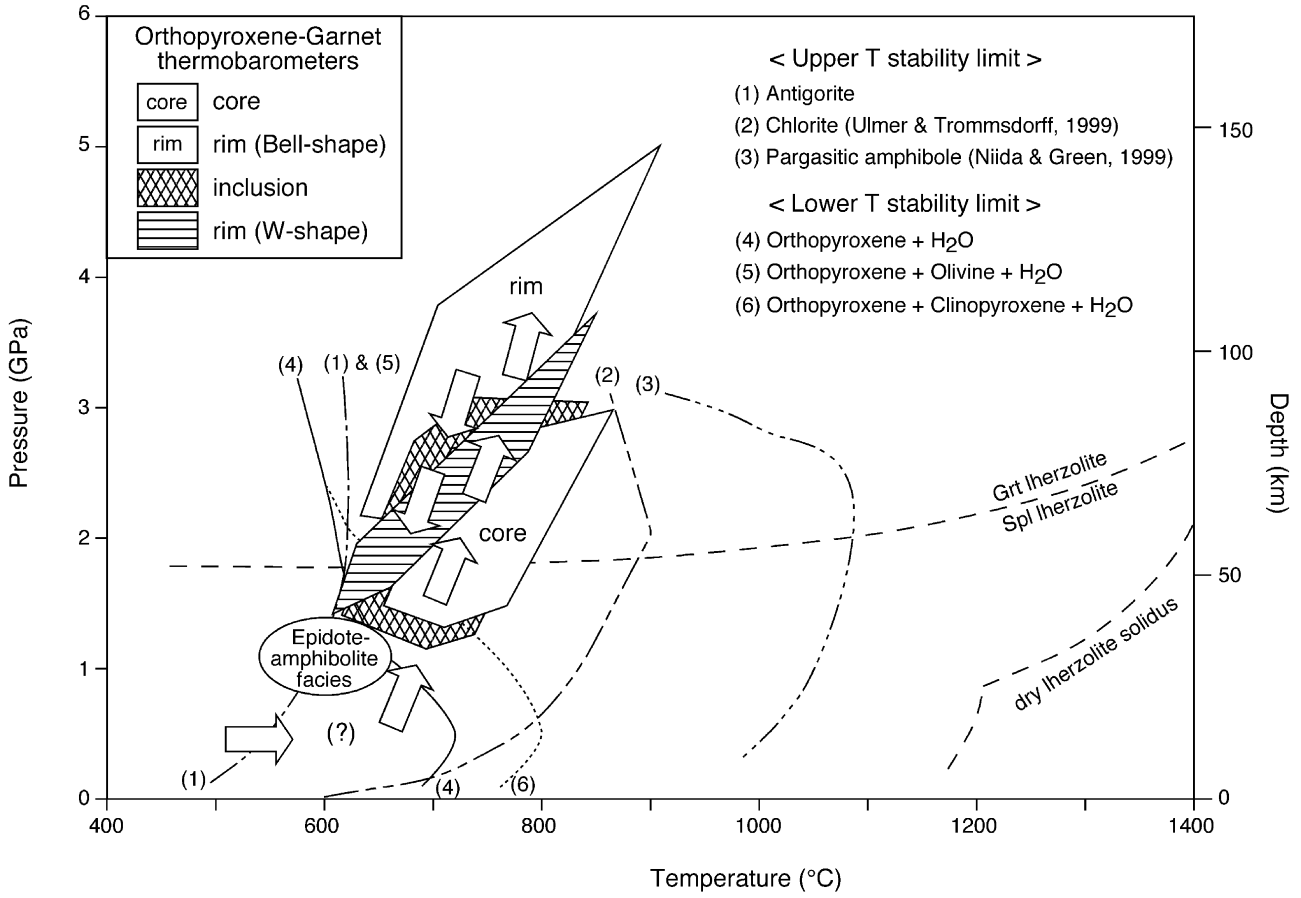

Fig. 13. Synoptic and generalized *P–T* trajectory for the GUM rocks from the Gongen area, Sanbagawa metamorphic belt. Stabilities of antigorite, orthopyroxene + H_2O, orthopyroxene + olivine + H_2O and orthopyroxene + clinopyroxene + H_2O are calculated using THERMOCALC Ver. 3.1 (Holland & Powell, 1998). The generic spinel peridotite–garnet peridotite transition and a dry lherzolite solidus are from Medaris (1999).

peak stage are 700–810 °C, similar to that of the early stage. The *P/T* ratio during the prograde stage is at least as high as 3.1 GPa/100 °C or greater.

The *P–T* conditions experienced during exhumation are locally recorded at the rims of some minerals. Chemical compositions at the interface between W-shaped Al zoned orthopyroxene and garnet give *P–T* conditions of 1.8–3.0 GPa/630–780 °C giving an indication of a *P–T* path during exhumation that has a slightly gentler *P/T* slope ($<$ 3.1 GPa/100 °C) than that of the prograde HP–UHP stage ($>$ 3.1 GPa/100 °C, Fig. 10a,c,e & f).

ORIGIN OF GONGEN GUM ROCKS AND GEODYNAMIC IMPLICATIONS

The presence of well developed layering in the Higashi-akaishi mass including chromitite, pyroxenite and garnet–clinopyroxenite layers (up to 1 m thick) contained within uniform dunite, the wide and systematic variation of bulk-rock compositions, and the common occurrence of metamorphosed peridotite–gabbro layered complexes throughout the Besshi region (Yokoyama, 1980; Kunugiza *et al.*, 1986) are evidence that the GUM rocks originated from former layered mafic and ultramafic intrusions. There are two possible origins for layered complexes in HP–UHP metamorphic terranes: (1) peridotite and pyroxenite differentiated from mantle-derived magma within the uppermost wedge mantle (case I in Fig. 14) and (2) ultramafic portions of crustal mafic-ultramafic complexes that were differentiated from mafic magma prior to subduction (case II in Fig. 14) (e.g. Brueckner & Medaris, 2000; Zhang *et al.*, 2000).

The discovery of amphibole, chlorite and magnetite inclusions in orthopyroxene and other silicates is an important petrological constraint on the origin of the GUM rocks. The inclusions suggest the importance of hydrous reactions under low temperature conditions. Such low-*T* inclusions are commonly thought to indicate an early stage of serpentinization and that the protoliths were oceanic lithospheric mantle (e.g. Brueckner & Medaris, 2000). Yang & Jahn (2000), however, reported low *P–T* assemblages (chlorite,

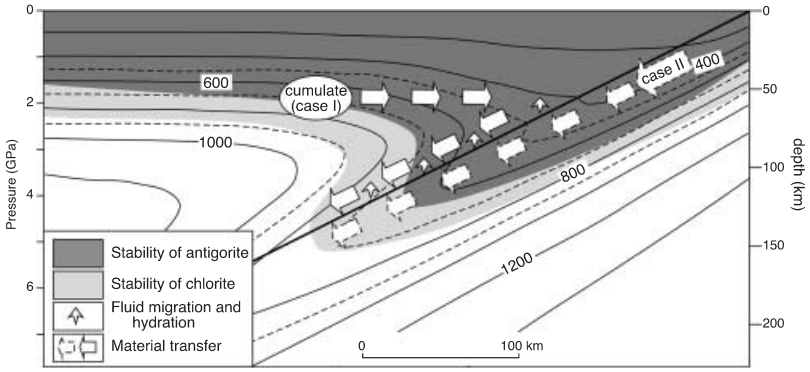

Fig. 14. Schematic two-dimensional diagram of a subduction zone showing two possible origins of GUM rocks from the Gongen area, Sanbagawa metamorphic belt. Thermal structure is from the numerical modelling of Peacock (1996) for steady-state subduction with the subducting plate velocity of 10 mm year^{-1} and shear heating component of 5%.

hornblende, Na-gedrite, Na-phlogopite, talc, etc.) included in garnet of initial mantle slices from the Sulu UHP terrane and put forth two hypotheses concerning crystallization of the inclusions: that the peridotites were (1) emplaced into the crust and infiltrated by crust-derived fluid or (2) convected from deep-seated mantle to the corner of mantle wedge and infiltrated by fluid migrating from the dehydrating slab. Although the occurrence of hydrous inclusions does not necessarily imply that the GUM rocks of the Gongen area are necessarily either equivalents of crustal peridotite as described by Brueckner & Medaris (2000) or Type B garnet peridotite described by Zhang *et al*. (2000), the GUM rocks have certainly experienced a low *P–T* environment at an earlier stage of prograde HP–UHP metamorphism.

The low *P–T* equilibrium conditions at an early stage and the steep *P/T* ratio of the prograde stage of the GUM rocks from the Gongen area trace a kinked, concave upwards, anticlockwise path. Such *P–T* paths are commonly documented from UHP terranes (Schertl *et al*., 1991; Reinecke, 1998; Enami & Nagasaki, 1999; Katayama *et al*., 2000), and are numerically simulated for subducted oceanic crust (Peacock, 1992; Bousquet *et al*., 1997). Thus, the kinked, concave upwards, *P–T* path is expected for ultramafic rocks of case II in Fig. 14. In the case I, the kinked prograde path is possibly attained during the process that the GUM rocks were dragged down parallel to the slab–wedge interface in the subduction zone.

CONCLUSIONS

The following conclusions are gained through our detailed petrological and mineralogical works on alpine-type GUM rocks in the Gongen area of the Sanbagawa metamorphic belt, central Shikoku.

(1) Garnet and orthopyroxene coexist as the main constituents of garnet clinopyroxenite, websterite and wehrlite in the layered ultramafic unit. Orthopyroxene coexisting with garnet commonly shows a bell-shaped Al zoning pattern with a continuous decrease of Al from core to rim. Estimated *P–T* conditions for the core and rim compositions of orthopyroxene are 1.5–2.4 GPa/700–800 °C and 2.9–3.8 GPa/700–810 °C, respectively, suggesting that the pressure gradient during prograde metamorphism was as high as > 3.1 GPa/100 °C. Chlorite, edenitic amphibole and magnetite occur as inclusions in orthopyroxene and other major silicate minerals. These low-*T* mineral inclusions imply that the GUM rocks experienced a low *P–T* environment at an early stage of prograde HP–UHP metamorphism.

(2) The low *P–T* equilibrium conditions at an early stage and the steep pressure gradient of the subsequent prograde metamorphism traces a kinked, concave upwards, prograde path similar to the *P–T* path reported from many UHP terranes. The inferred *P–T* trajectory can be attributed to (i) hydration of mantle cumulate by fluid migrating from the dehydrating slab and dragging down of the resulting rocks parallel to the slab–wedge interface in the subduction/collision zone or (ii) ocean floor metamorphism and/or serpentinization at early stage of subduction of oceanic lithosphere and ensuing HP–UHP prograde metamorphism. We cannot conclusively interpret the origin of the Gongen GUM rocks from their *P–T* trajectory deduced from petrological and mineralogical data alone. Geochemical and isotopic studies may help understand the petrogenesis of the UHP GUM rocks occurring in the HP metamorphic belt of an island arc (e.g. Jahn, 1998, 1999).

ACKNOWLEDGEMENTS

We thank C. Parkinson, J. A. Gilotti, S. Wallis and J. J. Yang for their constructive and critical reviews of this manuscript and to T. Itaya for his helpful comments. We acknowledge M. Brown for his editorial advice, S. Yogo for making many thin sections and M. Tsuboi for his assistance during XRF analyses. This study was financially supported by a Grant-in-Aid for Scientific Research from JSPS to M.E. (No. 14540448) and Fukada Geological Institute to T.M.

SUPPLEMENTARY MATERIAL

Table S1 is available online from http://www.blackwellpublishing.com/products/journals/suppmat/JMG/JMG492/JMG492sm.htm.

REFERENCES

Ai, Y., 1994. A revision of the garnet-clinopyroxene Fe^{2+}-Mg exchange geothermometer. *Contributions to Mineralogy and Petrology*, **115,** 467–473.

Altherr, R. & Kalt, A., 1996. Metamorphic evolution of ultra-high-pressure garnet peridotites from the Variscan Vosges Mts. (France). *Chemical Geology*, **134,** 27–47.

Aoya, M., 2001. P-T-D path of eclogite from the Sambagawa belt deduced from combination of petrological and microstructural analyses. *Journal of Petrology*, **42,** 1225–1248.

Bamba, T., 1953. The Higashi akaishi-yama dunite mass in Shikoku (studies on spinels associated with the ultra-mafic rocks, II). *Journal of the Geological Society of Japan*, **59,** 437–445 (in japanese with English abstract).

Banno, S., 1968. Some considerations on the crystallization temperature of eclogites in the Higashi-akaishi peridotite mass. *Journal of Japanese Association of Mineralogists, Petrologists and Economic Geologists*, **59,** 1–8 (in Japanese with English abstract).

Banno, S., 1970. Classification of eclogites in terms of physical conditions of their origin. *Physics of the Earth and Planetary Interiors*, **3,** 405–421.

Berman, R. G., Aranovich, L. Y. & Pattison, D. R. M., 1995. Reassessment of the garnet-clinopyroxene Fe-Mg exchange thermometer: II, Thermodynamic analysis. *Contributions to Mineralogy and Petrology*, **119,** 30–42.

Bertrand, P. & Mercier, J.-C. C., 1985. The mutual solubility of coexisting ortho- and clinopyroxene: toward and absolute geothermometer for the natural system? *Earth and Planetary Science Letters*, **76,** 109–122.

Bousquet, R., Goffè. B., Henry, P., Le Pichon, X. & Chopin, C., 1997. Kinematic, thermal and petrological model of the Central Alps: Lepontine metamorphism in the upper crust and eclogitisation of the lower crust. *Tectonophysics*, **273,** 105–127.

Brey, G. P. & Köhler, T., 1990. Geothermobarometry in four-phase lherzolites II. New thermobarometers, and practical assessment of existing thermobarometers. *Journal of Petrology*, **31,** 1353–1378.

Brueckner, H. K. & Medaris, L. G., 2000. A general model for the intrusion and evolution of 'mantle' garnet peridotites in high-pressure and ultra-high-pressure metamorphic terranes. *Journal of Metamorphic Geology*, **18,** 123–133.

Brueckner, H. K. & Medaris, L. G., 1998. A tale of two orogens: the contracting T-P-t history and geochemical evolution of mantle in high- and ultrahigh-pressure metamorphic terranes of the Norwegian Caledonides and the Czech Variscides. *Schweizerische Mineralogische und Petrographische Mitteilungen*, **78,** 293–307.

Carswell, D. A., 1991. The garnet-orthopyroxene Al barometer: problematic application to natural garnet lherzolite assemblages. *Mineralogical Magazine*, **55,** 19–31.

Carswell, D. A. & Harley, S. L., 1990. Mineral barometry and thermometry. In: *Eclogite Facies Rocks* (ed. Carswell, D. A.), pp. 83–110. Blackie, Glasgow.

Carswell, D. A., Harvey, M. A. & Al-Samman, A., 1983. The petrogenesis of contrasting Fe-Ti and Mg-Cr garnet peridotite types in the high grade gneiss complex of western Norway. *Bulletin de Minèralogie*, **106,** 727–750.

Enami, M., 1983. Petrology of pelitic schists in the oligoclase-biotite zone of the Sanbagawa metamorphic terrain, Japan: phase equilibria in the highest grade zone of a high-pressure intermediate type of metamorphic belt. *Journal of Metamorphic Geology*, **1,** 141–161.

Enami, M. & Nagasaki, A., 1999. Prograde P-T path of kyanite eclogites from Junan in the Su-Lu ultrahigh-pressure province, eastern China. *Island Arc*, **8,** 459–474.

Enami, M., Wallis, S. R. & Banno, Y., 1994. Paragenesis of sodic pyroxene-bearing quartz schists: implications for the P-T history of the Sanbagawa belt. *Contributions to Mineralogy and Petrology*, **116,** 182–198.

Ernst, W. G., 1978. Petrochemical study of lherzolitic rocks from the Western Alps. *Journal of Petrology*, **19,** 341–353.

Ernst, W. G. & Liu, J., 1998. Experimental phase-equilibrium study of Al- and Ti-contnets of calcic amphibole in MORB – A semiquantitative thermobarometer. *American Mineralogist*, **83,** 952–969.

Ernst, W. G., Onuki, H., Seki, Y. & Gilbert, M. C., 1970. *Comparative Study of Low-Grade Metamorphism in the California Coast Ranges and the Outer Metamorphic Belt of Japan.* Geological Society of America Memoir 124, pp. 276, Boulder, USA.

Evans, B. W. & Trommsdorff, V., 1978. Petrogenesis of garnet lherzolite, Cima di Gagnone, Lepontine Alps. *Earth and Planetary Science Letters*, **40,** 333–348.

Harley, S. L., 1984a. An experimental study of the partitioning of Fe and Mg between garnet and orthopyroxene. *Contributions to Mineralogy and Petrology*, **86,** 359–373.

Harley, S. L., 1984b. The solubility of alumina in orthopyroxene coexisting with garnet in FeO-MgO-Al_2O_3-SiO_2 and CaO-FeO-MgO-Al_2O_3-SiO_2. *Journal of Petrology*, **25,** 665–696.

Harley, S. L. & Green, D. H., 1982. Garnet-orthopyroxene barometry for granulites and peridotites. *Nature*, **300,** 697–701.

Higashino, T., 1990. The higher-grade metamorphic zonation of the Sambagawa metamorphic belt in central Shikoku, Japan. *Journal of Metamorphic Geology*, **8,** 413–423.

Holland, T. J. B. & Powell, R., 1998. An internally consistent thermodynamic data set for phases of petrological interest. *Journal of Metamorphic Geology*, **16,** 309–343.

Horikoshi, G., 1937. On the eclogite in the vicinity of Higashi-akaishi-yama in the province of Iyo. *Journal of Geological Society of Japan*, **44,** 141–144 (in Japanese).

Itaya, T., Brothers, R. N. & Black, P. M., 1985. Sulfides, oxides and sphene in high-pressure schists from New Caledonia. *Contributions to Mineralogy and Petrology*, **91,** 151–162.

Jahn, B.-M., 1998. Geochemical and isotopic characterstics of UHP eclogites and ultramafic rocks of the Dabie orogen: Implications for continental subduction and collisional tectonics. In: *When Continents Collide: Geodynamics and Geochemistry of Ultrahigh-Pressure Rocks* (eds Hacker, B. & Liou, J. G.), pp. 203–239, Kluwer, Dordrecht.

Jahn, B. M., 1999. Sm-Nd isotope tracer study of UHP metamorphic rocks: Implications for continental subduction and collisional tectonics. *International Geology Review*, **41,** 859–885.

Jamtveit, B., 1987. Metamorphic evolution of the Eiksunddal eclogite complex, western Norway, and some tectonic implications. *Contributions to Mineralogy and Petrology*, **95,** 82–99.

Kadarusman, A. & Parkinson, C. D., 2000. Petrology and *P-T* evolution of garnet peridotites from central Sulawesi, Indonesia. *Journal of Metamorphic Geology*, **18,** 193–209.

Katayama, I., Zayachkovsky, A. A. & Maruyama, S., 2000. Prograde pressure-temperature records from inclusions in zircons from ultrahigh-pressure-high-pressure rocks of the Kokchetav Massif, northern Kazakhstan. *Island Arc*, **9,** 417–427.

Kretz, R., 1983. Symbols for rock-forming minerals. *American Mineralogist*, **68,** 277–279.

Krogh Ravna, E., 2000. The garnet-clinopyroxene Fe^{2+}-Mg geothermometer: An updated calibration. *Journal of Metamorphic Geology*, **18,** 211–219.

Krogh, E. J. & Carswell, D. A., 1995. HP and UHP eclogites and garnet peridotites in the Scandinavian Caledonides. In: *Ultrahigh Pressure Metamorphism* (eds Coleman, R. G. & Wang, X.), pp. 244–298. Cambridge University Press, Cambridge.

Kugimiya, Y. & Takasu, A., 2002. Geology of the Western Iratsu mass within the tectonic melange zone in the Sambagawa metamorphic belt, Besshi district, central Shikoku, Japan. *Journal of Mineralogical Society of Japan*, **108,** 644–662 (in Japanese with English abstract).

Kunugiza, K., 1980. Dunites and serpentinites in the Sanbagawa metamorphic belt, central Shikoku and Kii Peninsula, Japan. *Journal of Japanese Association of Mineralogists, Petrologists and Economic Geologists*, **76,** 14–24.

Kunugiza, K., 1981. Two contrasting types of zoned chromite of the Mt. Higashi-Akaishi peridotite body of the Sanbagawa metamorphic belt, central Shikoku. *Journal of Japanese Association of Mineralogists, Petrologists and Economic Geologists*, **76,** 331–342.

Kunugiza, K., 1984. Metamorphism and origin of ultramafic bodies of the Sanbagawa metamorphic belt in central Shikoku. *Journal of Japanese Association of Mineralogists, Petrologists and Economic Geologists*, **79,** 20–32 (in Japanese with English abstract).

Kunugiza, K., Takasu, A. & Banno, S., 1986. The origin and metamorphic history of the ultramafic and metagabbro bodies in the Sanbagawa metamorphic belt. In: *Blueschists and Eclogites* (eds Evans, B. E. & Brown, E. H.) Memoir, pp. 375–385, Geological Society of America, Boulder CO.

Leake, B. E., Woolley, A. R., Arps, C. E. S., *et al*., 1997. Nomenclature of amphiboles: Report of the subcommittee on amphiboles of the International Mineralogical Association Commission on new minerals and mineral names. *Mineralogical Magazine*, **61,** 295–321.

Liu, J., Bohlen, S. R. & Ernst, W. G., 1996. Stability of hydrous phases in subducting oceanic crust. *Earth and Planetary Science Letters*, **143,** 161–171.

Medaris, L. G., 1999. Garnet peridotites in Eurasian high-pressure and ultrahigh-pressure terranes: a diversity of origins and thermal histories. *International Geology Review*, **41,** 799–815.

Medaris, L. G. J., Beard, B. L., Johnson, C. M., Valley, J. W., Spicuzza, M. J., Jelinek, E. & Misar, Z., 1995. Garnet pyroxenite and eclogite in the Bohemian Massif: geochemical evidence for Variscan recycling of subducted lithosphere. *Geologische Rundschau*, **84,** 489–505.

Mengel, K. & Green, D. H., 1989. Stability of amphibole and phlogopite in metamomatized peridotite under water-saturated and water-undersaturated conditions. In: *Kimberlites and Related Rocks*, Vol. 1. Their Composition**,** Occurrence, Origin and Emplacement. (eds Ross, J. A., Jaques, A. L., Ferguson, J., *et al*.), Geological Society of Australia Special Publication 14, pp. 571–581, Victoria.

Miyashiro, A., 1961. Evolution of metamorphic belts. *Journal of Petrology*, **2,** 277–331.

Miyashiro, A., 1994. *Metamorphic Petrology*, pp. 404. UCL Press, London.

Mori, T., 1972. MS. Petrology of the Mt. Higashi-akaishi peridotite and garnet clinopyroxenite, S.W. Japan. *Unpub. Master Thesis*, *Kanazawa University, Kanazawa*.

Mori, T. & Banno, S., 1973. Petrology of peridotite and garnet clinopyroxenite of the Mt. Higashi-Akaishi mass, Central Sikoku, Japan – Subsolidus relation of anhydrous phases. *Contributions to Mineralogy and Petrology*, **41,** 301–323.

Nickel, K. G. & Green, D. H., 1985. Empirical geothermobarometry for garnet peridotites and implications for the nature of the lithosphere, kimberlites and diamonds. *Earth and Planetary Science Letters*, **73,** 158–170.

Niida, K. & Green, D. H., 1999. Stability and chemical composition of pargasitic amphiboles in MORB pyrolite under upper mantle conditions. *Contributions to Mineralogy and Petrology*, **135,** 18–40.

Nimis, P. & Taylor, W. R., 2000. Single clinopyroxene thermobarometry for garnet peridotites. Part I. Calibration and testing of a Cr-in Cpx barometer and an enstatite-in Cpx thermometer. *Contributions to Mineralogy and Petrology*, **139,** 541–554.

O'Neill, H. S. C. & Wood, B. J., 1979. An experimental study of Fe-Mg partitioning between garnet and olivine and its calibration as a geothermometer. *Contributions to Mineralogy and Petrology*, **70,** 59–70.

O'Neill, H. S. C. & Wood, B. J., 1980. An experimental study of Fe-Mg partitioning between garnet and olivine and its calibration as a geothermometer, corrections. *Contributions to Mineralogy and Petrology*, **72,** 337.

Peacock, S. M., 1992. Blueschist-facies metamorphism, shear heating, and P-T-t paths in subduction shear zones. *Journal of Geophysical Research*, **97,** 17693–17707.

Peacock, S. M., 1996. Thermal and petrologic structure of subduction zones. In: *Subduction, Top to Bottom*. (eds Bebout, G. E., Scholl, D. W., Kirby, S. H. & Platt, J. P.), pp. 119–133, American Geophysical Union, Washington DC.

Reinecke, T., 1998. Prograde high- to ultrahigh-pressure metamorphism and exhumation of oceanic sediments at Lago di Cignana, Zermatt-Saas Zone, Western Alps. *Lithos*, **42,** 147–189.

Schertl, H.-P., Schreyer, W. & Chopin, C., 1991. The pyropecoesite rocks and their country rocks at Parigi, Dora Maira Massif, Western Alps: detailed petrography, mineral chemistry and PT-path. *Contributions to Mineralogy and Petrology*, **108,** 1–21.

Sen, S. K. & Bhattacharya, A., 1984. An orthopyroxene-garnet thermometer and its application to the Madras charnockites. *Contributions to Mineralogy and Petrology*, **88,** 64–71.

Takasu, A., 1989. P-T histories of peridotite and amphibolite tectonic blocks in the Sanbagawa metamorphic belt, Japan. In: *The Evolution of Metamorphic Belts* (eds Daly, J. S., Cliff, R. A. & Yardley, B. W. D.), pp. 533–538. Blackwell Scientific Publications, Oxford.

Taylor, W. R., 1998. An experimental test of some geothermometer and geobarometer formulations for upper mantle peridotites with application to the thermobarometry of fertile lherzorite and garnet websterite. *Neues Jahrbuch für Mineralogie Abhandlungen*, **172,** 381–408.

Tsujimori, T., Tanaka, C., Sakurai, T., *et al*., 2000. Illustrated introduction to eclogite in Japan. *Bulletin of Research Institute of Natural Sciences, Okayama University of Science*, **26,** 19–40.

Ulmer, P. & Trommsdorff, V., 1999. Phase relations of hydrous mantle subducting to 300 km. In: *Mantle Petrology: Field Observations and High-Pressure Experimentation: a Tribute to Francis R. (Joe) Boyd* (eds Fei, Y., Bertka, C. M. & Mysen, B. O.), pp. 259–281. The Geochemical Society, Houston, USA.

Wallace, M. E. & Green, D. H., 1991. The effect of bulk rock composition on the stability of amphibole in the upper mantle: implications for solidus positions and mantle metasomatism. *Mineralogy and Petrology*, **44,** 1–19.

Wallis, S. & Aoya, M., 2000. A re-evaluation of eclogite facies metamorphism in SW Japan: Proposal for an eclogite nappe. *Journal of Metamorphic Geology*, **18,** 653–664.

Wallis, S., Takasu, A., Enami, M. & Tsujimori, T., 2000. Eclogite and related metamorphism in the Sanbagawa belts, Southwest Japan. *Bulletin of Research Institute of Natural Sciences, Okayama University of Science*, **26,** 3–17.

Yamaguchi, M. & Oshima, T., 1977. Variation of rock facies in the Higashi-Akaishi-yama ultramafic mass, Shikoku, Japan. *Science Reports of the Faculty of Science, Kyushu University, Geology*, **12,** 255–262 (in Japanese with English abstract).

Yang, J. J. & Jahn, B. M., 2000. Deep subduction of mantle-derived garnet peridotites from the Su-Lu UHP metamorphic terrane in China. *Journal of Metamorphic Geology*, **18,** 167–180.

Yokoyama, K., 1974. MS. Petrogenesis of the Higashi-akaishi peridotite and Iratsu epidote amphibolite. *Unpub. Master Thesis*, *Kanazawa University, Kanazawa*.

Yokoyama, K., 1975. Garnet lamellae in clinopyroxene from the Mt. Higashi-akaishi peridotite mass, central shikoku. *Journal of Geological Society of Japan*, **81,** 431–463.

Yokoyama, K., 1980. Nikubuchi peridotite body in the Sanbagawa metamorphic belt; Thermal history of the 'Al-pyroxene-rich suite' peridotite body in high pressure metamorphic terrain. *Contributions to Mineralogy and Petrology*, **73,** 1–13.

Zhang, R. Y., Liou, J. G. & Cong, B., 1994. Petrogenesis of garnet-bearing ultramafic rocks and associated eclogites in the Su-Lu ultrahigh-P metamorphic terrane, eastern China. *Journal of Metamorphic Geology*, **12,** 169–186.

Zhang, R. Y., Liou, J. G., Yang, J. S. & Yui, T. F., 2000. Petrochemical constraints for dual origin of garnet peridotites from the Dabie-Sulu UHP terrane, eastern-central China. *Journal of Metamorphic Geology*, **18,** 149–166.

Received 23 December 2002; revision accepted 14 September 2003.